Electronic Supplementary Information for

Thiadiazole-Based Covalent Triazine Framework Nanosheet for Highly Selective and Sensitive Primary Aromatic Amines Detection among Various Amines

Yuanzhe Tang,[a,b] *Hongliang Huang,**[a,b] *Ben Peng,*[a,b] *Yanjiao Chang,*[a,b] *Yang Li*[a,b] *and Chongli Zhong**[a,b,c]

[a] State Key Laboratory of Separation Membranes and Membrane Processes, Tiangong University, Tianjin 300387, China

[b] School of Chemistry and Chemical Engineering, Tiangong University, Tianjin 300387, China.

[c] College of Chemical Engineering, Beijing University of Chemical Technology, Beijing 100029, China

E-mail: huanghongliang@tiangong.edu.cn, zhongchongli@tiangong.edu.cn

Experimental section

Materials

The various organic amines, cesium carbonate (Cs_2CO_3), potassium carbonate (K_2CO_3), $LiN(SiMe_3)_2$, benzene-1,4-dicarbonitrile, 4-formylphenylboronic acid, tetrakis(triphenylphosphine)palladium $Pd(PPh_3)_4$ and 4,7-Dibromobenzo[c][1,2,5]thiadiazole were purchased from Energy Chemical Co. Ltd. Hydrochloric acid (HCl) and acetone were purchased from Beijing Chemical Works. Dimethyl sulfoxide (DMSO), diethyl ether (Et_2O), ethanol (EtOH), methanol (MeOH), dichloromethane (DCM), N, N-Dimethylformamide (DMF) and Tetrahydrofuran (THF) were purchased from Sinopharm Chemical Reagent Co. Ltd.

Equipment

FT-IR Spectra were collected on a FT-IR spectrometer equipped with an ATR attachment (TENSOR II, Bruker, Germany) over the wavenumber range of 400-4000 cm^{-1}. ^1H Nuclear magnetic resonance (NMR) spectra were measured on a Bruker AVANCE III 400M spectrometer. Solid-state ^{13}C-NMR spectra were recorded at room temperature on a Bruker Fourier 300 M spectrometer. X-ray photoelectron spectroscopy (XPS) was measured on a Thermofisher K-alpha XPS spectrometer. High resolution transmission electron microscopy (HR-TEM) micrographs were recorded on JEM-2100F (JEOL, Japan). Atomic-force microscopy (AFM) images were collected by a scanning probe microscope (Bruker Dimension ICON, USA). The pore properties of the samples were measured by N_2 adsorption and desorption at 77 K using ASAP 2020 Plus HD88. Thermogravimetric analysis (TGA) data were obtained by using a NETZSCH TG 209 F3 Tarsus analyzer with a heating rate of 10 °C min^{-1} under N_2 atmosphere. Fluorescence spectra data were recorded on an F-7000 Fluorescence spectrophotometer equipped with a xenon lamp and quartz carrier. Fluorescence decay curves and fluorescent absolute quantum yield of the samples were measured at ambient temperature using an Edinburgh FLS 980 spectrometer

(Edinburgh Instruments, UK). UV−vis spectra were obtained with a UV-2600 spectrophotometer in the range of 250−800 nm at room temperature. Powder X-ray diffraction data (PXRD) analysis of powders were recorded on a SHIMADZU XRD-6000-X-ray diffractometer in reflection mode using Cu Ka radiation (λ=1.5406 Å). The 2θ range from 1˚ to 50˚ was scanned with a step size of 0.01˚. UV−vis spectra were recorded on a Shimadzu UV-2600 spectrometer.

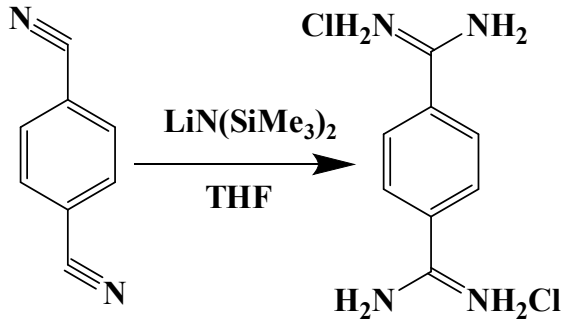

Scheme S1. Synthetic procedure for PAHC monomer.

Synthesis of phenamidine hydrochloride (PAHC). PAHC monomer was synthesized according to the published literatures[1,2] To a 1000 mL single-necked, round-bottomed flask, benzene-1,4-dicarbonitrile (6.4 g, 50.0 mmol) and THF (100 mL) were added, which was degassed with three freeze-vacuum-thaw cycles in N_2. $LiN(SiMe_3)_2$ solution (1M, 200 mL) was added dropwise in the mixture within 30 min at ice-water bath. The mixture was stirred at room temperature for 3 h and then cooled to 0 °C. Then HCl–EtOH mixture (6M, 200 mL) was carefully added the reaction system. After standing overnight, the white precipitate was filtered, washed with Et_2O, and then recrystallized from H_2O–EtOH mixture. Yield: (2.26 g, 96%).

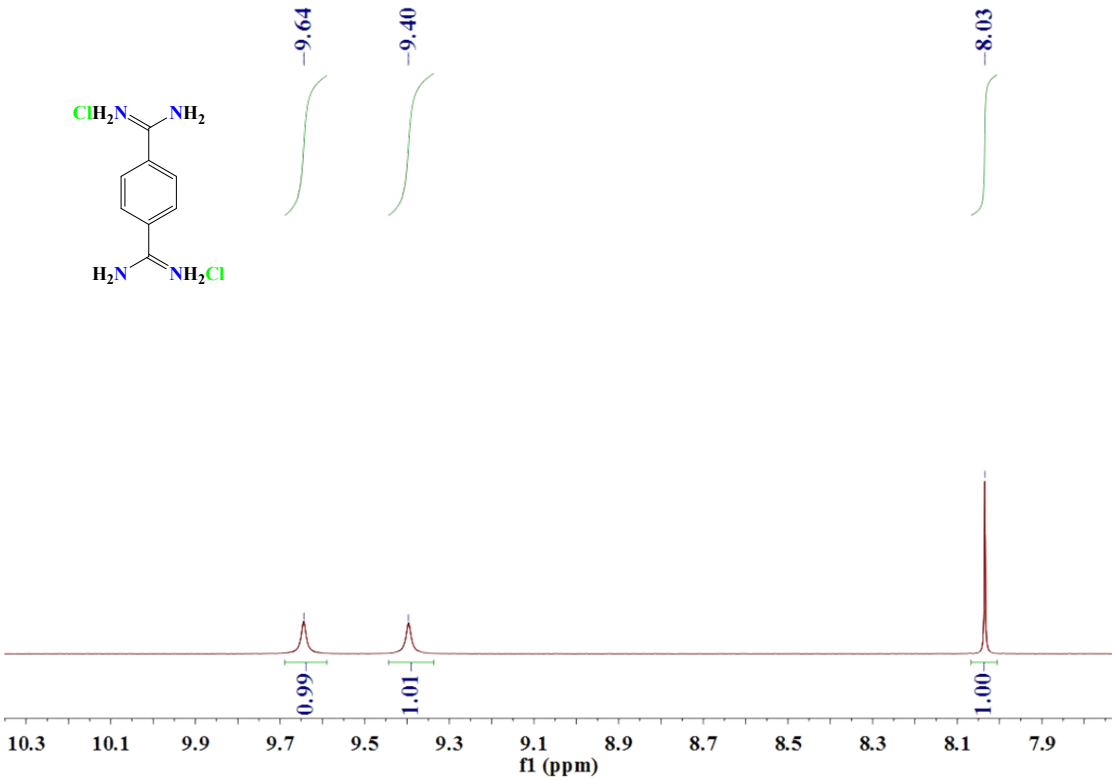

Fig. S1 ^{1}H-NMR of PAHC monomer.

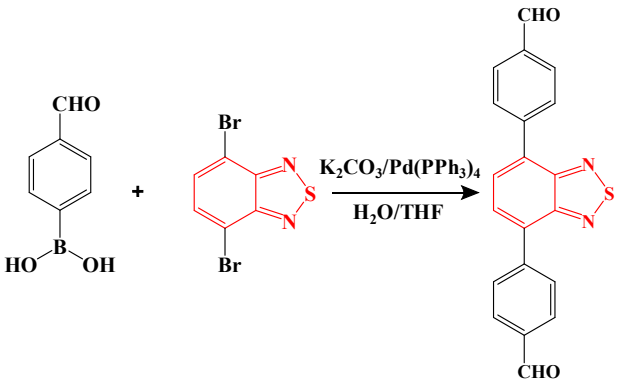

Scheme S2. Synthetic procedure for BTDD monomer.

Synthesis of 4, 4'-(benzothiadiazole-4,7-diyl)dibenzaldehyde (BTDD).

To a 1000 mL three-necked, round-bottomed flask, 4,7-dibromo-2,1,3-benzothiadiazole (17 mmol, 5g), 4-formylphenylboronic acid (51 mmol, 7.65 g), K_2CO_3 (100 mmol, 13.9g), H_2O (50 mL), THF (600 mL), and $Pd(PPh_3)_4$ (0.12 g) was added. Under the protection of nitrogen, the suspension was reacted with stirring at reflux for 48 h. The organic solvent was evaporated on rotary evaporator. After that,

the crude product was extracted with DCM. The organic phase was dried with $MgSO_4$. After removed the DCM solvent, the crude product was column chromatographed over silica gel using pure dichloromethane to the product as yellow solid. (5.18 g, 88% yield).

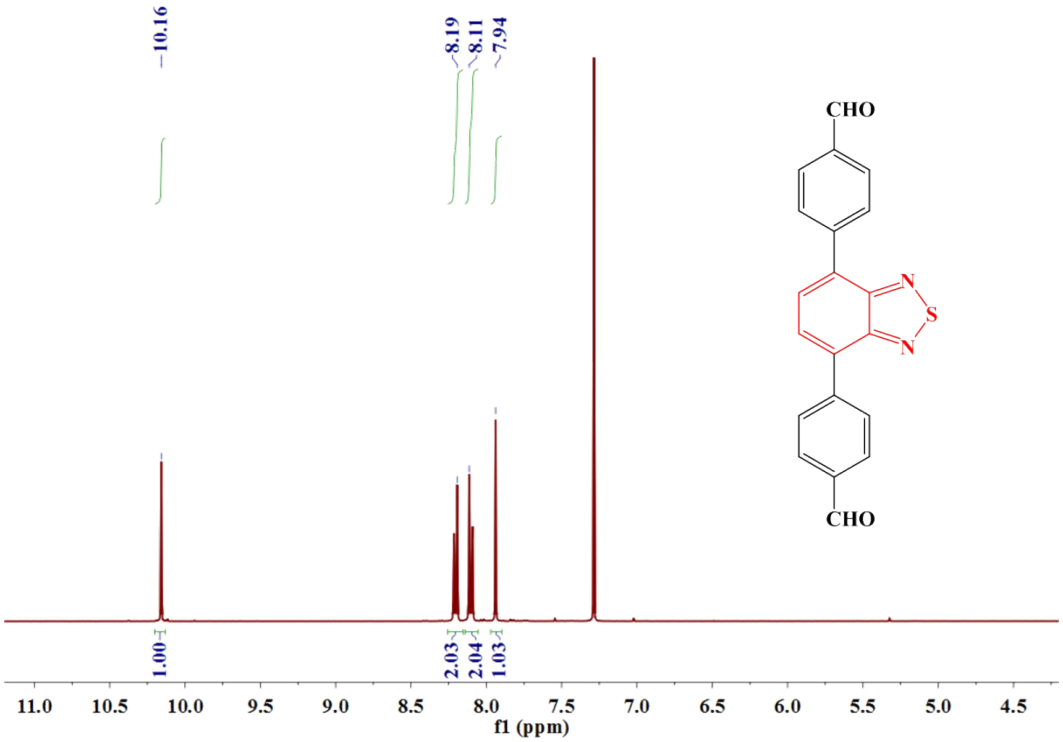

Fig. S2 ^{1}H-NMR of BTDD monomer.

Synthesis of F-CTF-3. In a 100 mL single-necked, round-bottomed flask, BTDD (172 mg, 0.5 mmol), PAHC (235.2 mg, 1.0 mmol), and cesium carbonate (716.8 mg, 2.2 mmol), DMSO (50 mL) and H_2O (2 mL) were added. The mixture was heated at 60 °C for 12 h, then heated at 80 °C, 100 °C for 12 h and 120 °C for 3 days to yield a yellow solid. The resulting solid was washed with dilute HCl (3 × 100 mL), water (3 × 100 mL), acetone (3 × 100 mL), and THF (3 × 100 mL), the obtained yellow solid was dried at 80 °C under vacuum for 12 h. (374.6 mg, 92% yield).

Fluorescence detection.

In a typical fluorescence detection experiment, 10 mg of F-CTF-3 sample was weighed, finely grounded, and then added to a cuvette containing 20 mL of deionized water under stirring. The fluorescence upon excitation at 372 nm of 2 ml F-CTF-3

suspension was measured in situ after increased addition of freshly prepared analyte solutions (3 mM, 20 μL addition each time). The mixed solution was stirred about 10 s to maintain its homogeneity and then the emission spectra were recorded at the excitation wavelength of 372 nm.

Similarly, in a selective detection experiment, 10 mg finely grounded F-CTF-3 sample was added to a cuvette containing 20 mL of deionized water under stirring. Fluorescence of the obtained 2 ml F-CTF-3 suspension was recorded. Then, 3 mM PAAs and saturated non-PAAs amines aqueous solutions were alternatively introduced (twice for each) into the suspension in such a sequence (In the case of PA-TPA): TPA (20 μL), TPA (20 μL), TPA (20 μL), TPA (20 μL), TPA (20 μL), TPA (20 μL), etc., the process was repeated until the total volume of added analytes solutions reached 200 μL. After each addition, the fluorescence of the suspension was monitored.

In addition, in a time-depended detection experiment, 10 mg finely grounded F-CTF-3 was added into a cuvette containing 20 mL of deionized water under stirring. Fluorescence of the obtained 2 ml F-CTF-3 suspension was recorded. Then, PAAs (20 μL) was added into the F-CTF-3 suspension and the mixture was shaken for a certain time before emission spectra measurements. For each point-in-time, the fluorescence intensity of the F-CTF-3 suspension was monitored.

Limit of detection (LOD) calculation

Combined the standard deviation (S_b) of fluorescence intensity detected in water for 20 times and the K_{sv} value calculated by Stern - Volmer (SV) equation, the LOD value was calculated by the following equation. [1,3,4]

$$S_b = \sqrt{\frac{\sum\left(1 - \frac{I_0}{I_1}\right)^2}{N-1}} (N = 20)$$

$$LOD = \frac{3S_b}{K_{SV}}$$

where S_b is the standard deviation for replicating detections of blank F-CTF-3 solutions; I_0 is the fluorescence intensity of F-CTF-3 in water; I_1 is the average of the I_0.

Regeneration of F-CTF-3. The F-CTF-3 used in detection measurements were collected and washed with DMF and acetone through stirring at room temperature for 12 h. This procedure was repeated at least three times by using fresh DMF and acetone. After filtration, the regenerated product was dried under vacuum at 333 K for 4 h to remove the residual solvents.

Dynamic/static quenching of F-CTF-3.

To investigate the quenching process between F-CTF-3 and the analyte, the nature of the quenching mechanism was explored using the Stern–Volmer (SV) equation: [5]

$$\frac{I_0}{I} = 1 + K_{sv}[Q] = 1 + K_q\tau_0[Q]$$

where I_0 and I are the fluorescence emission intensities of the F-CTF-3 in the absence and presence of the analyte; [Q] is the concentration of analyte; τ_0 is the average life of F-CTF-3 with the value about 1.67 ns; K_q is the rate constant in the process of double molecules quenching; K_{sv} is the dynamic quenching constant.

When $K_q < 2.0\times10^{10}$ mol/s, it can be determined that the quenching process is dynamic quenching;

When $K_q > 2.0\times10^{10}$ mol/s, the quenching process is the static quenching one.

Binding constants and stoichiometry

The binding constant (K_b) and the corresponding stoichiometry (n) were calculated

for each interaction between F-CTF-3 and analyte using the following equation[6]:

$$\log\left(\frac{I_0 - I}{I}\right) = logK_b + nlog[Q]$$

where I_0 and I are the fluorescence intensities of the F-CTF-3 in the absence and presence of different concentrations of analyte, respectively; [Q] is the concentration of the respective analyte; K_b is the binding constant and n is the stoichiometry of binding.

Adsorption kinetic experiment.

After pre-degassing F-CTF-3 sample (10 mg) was totally activated and then transferred into water PAA solutions with different schedule times in a vial, respectively. UV-vis spectra of the solutions were recorded to characterize the adsorption performances of F-CTF-3 along with the soaking time at 298 K. The amount of the PAAs adsorbed on the F-CTF-3 was calculated using the following equation:

$$Q_e = \frac{(C_0 - C_e)}{M} V$$

Where Q_e (mM g^{-1}) is the equilibrium adsorbed amount; C_0 and C_e (mM) are the initial and equilibrium concentrations of solution; V (L) is the volume of solution; and M (g) is the mass of F-CTF-3.

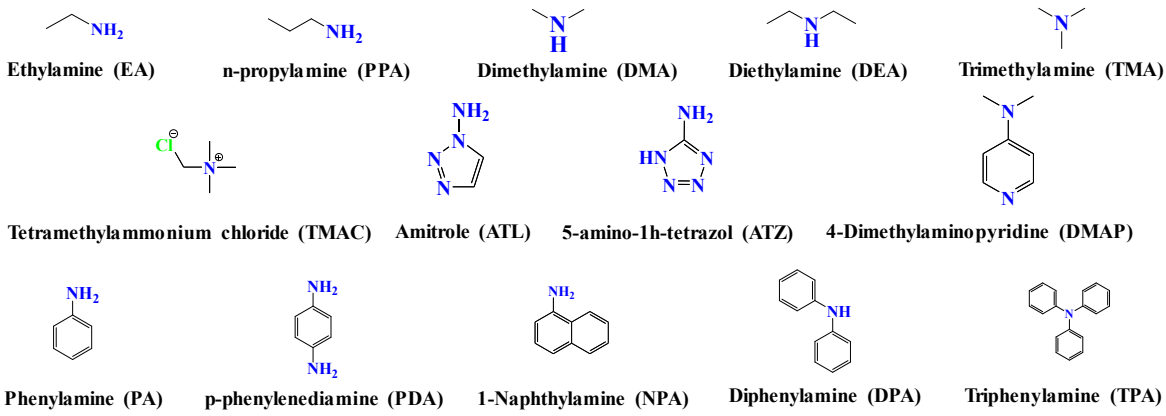

Fig. S3 Molecular structures of the various organic amines.

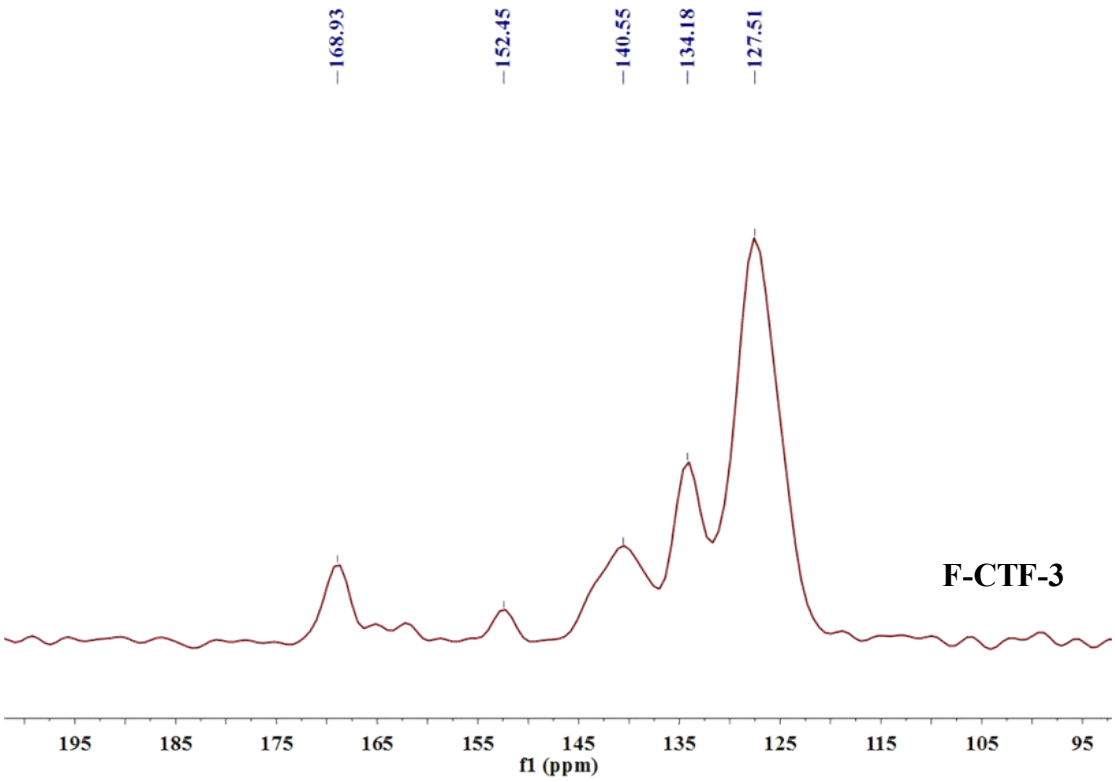

Fig. S4 ^{13}C-CPMAS solid-state NMR spectra of F-CTF-3.

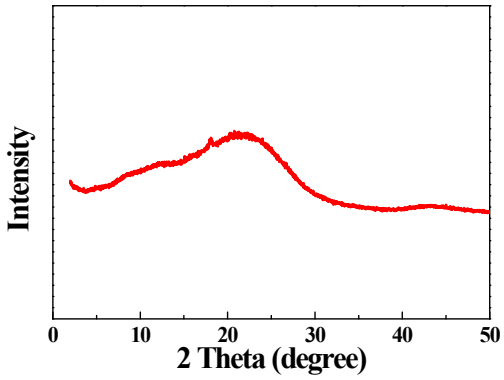

Fig. S5 XRD patterns of F-CTF-3.

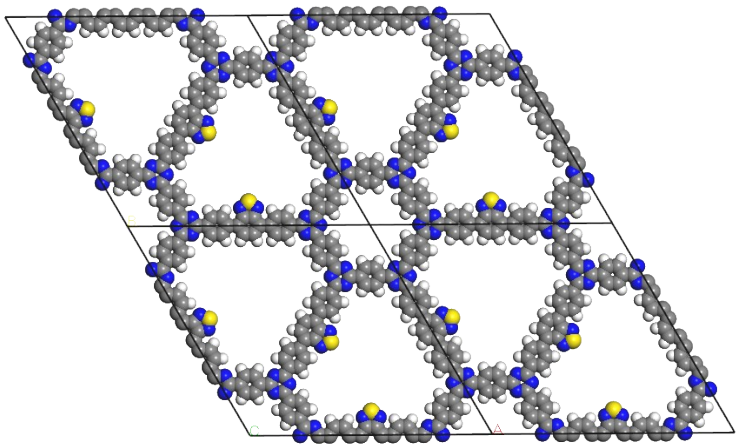

Fig. S6 Simulated AA stacking model structure of F-CTF-3 by Material Studios.

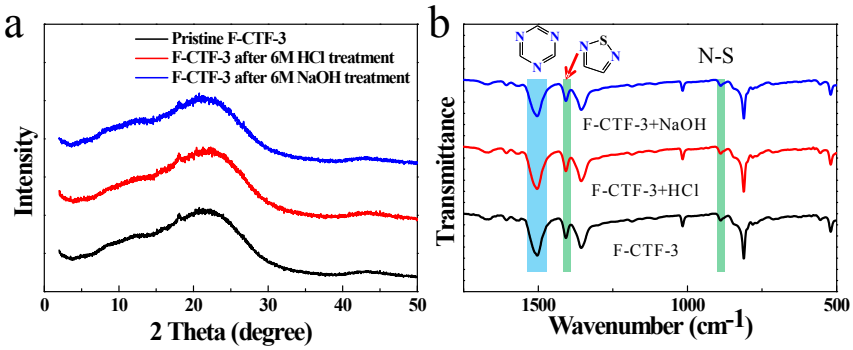

Fig. S7 (a) XRD patterns and (b) FT-IR spectra of F-CTF-3 before and after treated in NaOH (6M) and HCl (6M) aqueous solution, respectively.

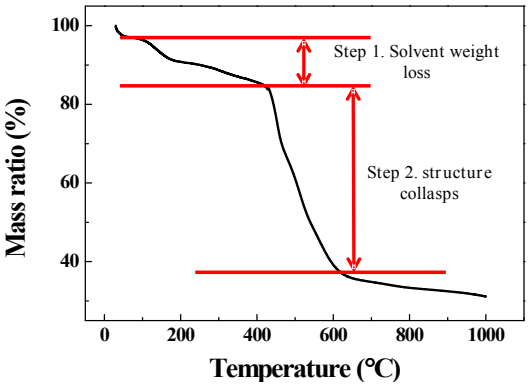

Fig. S8 TGA curves of as-prepared F-CTF-3.

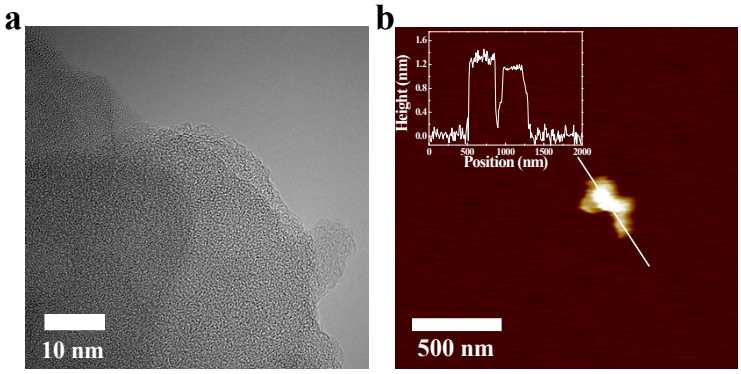

Fig. S9 (a). High-resolution TEM image of F-CTF-3. (b). AFM image and height profile of F-CTF-3.

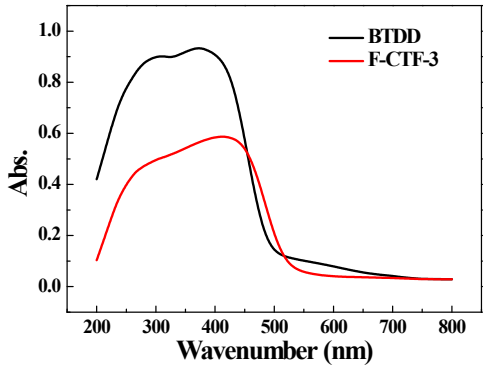

Fig. S10 Solid-state UV spectra of BTDD and F-CTF-3 excited at 372 nm and 412 nm, respectively.

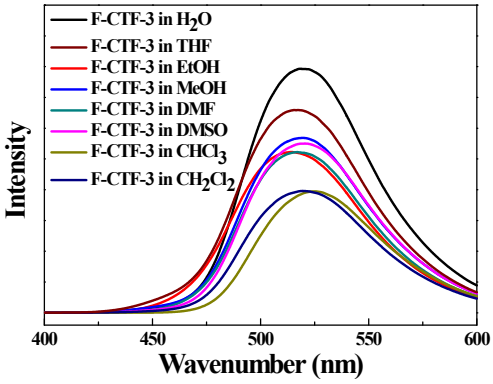

Fig. S11 Photoluminescent spectra of F-CTF-3 dispersed in different solvents excited at 416 nm in room temperature.

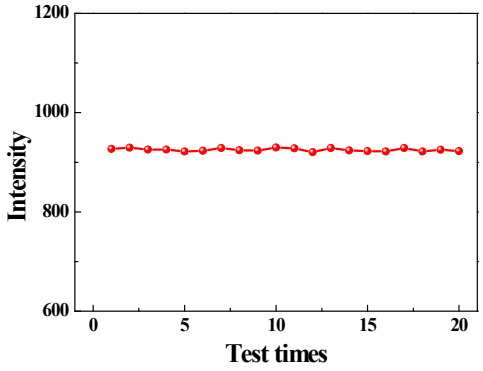

Fig. S12 Stability test for the fluorescence intensity of F-CTF-3 in water at room temperature.

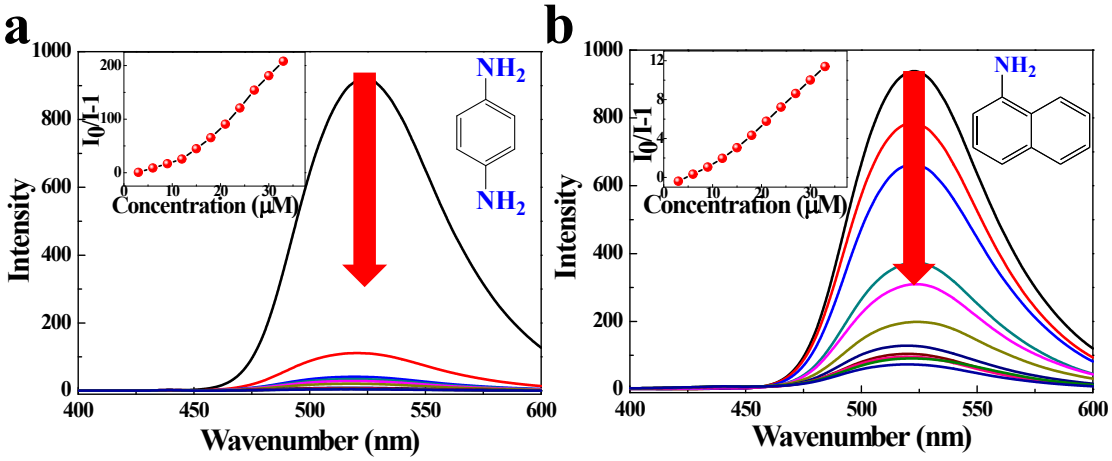

Fig. S13 The emission spectra of F-CTF-3 dispersed in water upon the increased addition of 200 μL (3 μM, 20 μL addition each time) aqueous solution of (a) PDA and (b) NPA at room temperature, respectively.

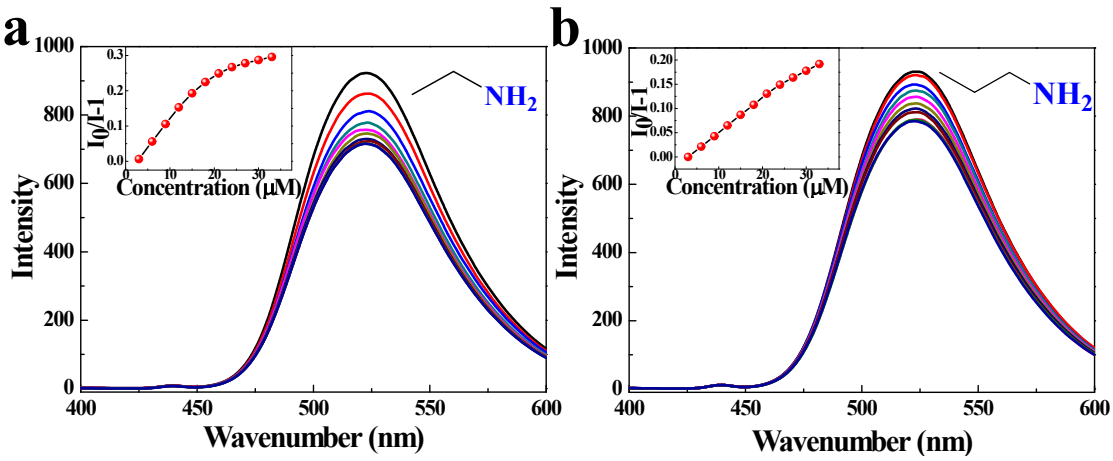

Fig. S14 The emission spectra of F-CTF-3 dispersed in water upon the increased addition of 200 μL (3 μM, 20 μL addition each time) aqueous solution of (a) EA and (b) PPA at room temperature, respectively.

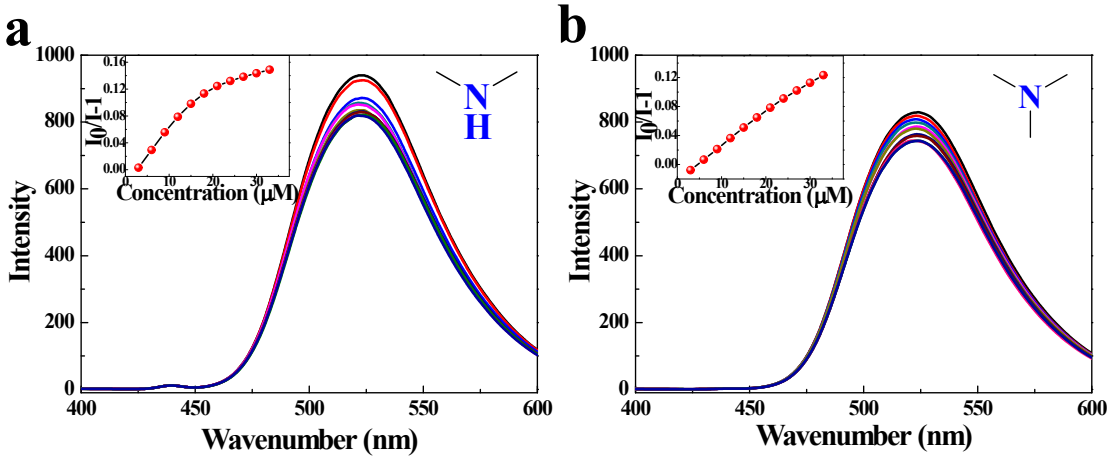

Fig. S15 The emission spectra of F-CTF-3 dispersed in water upon the increased addition of 200 μL (3 μM, 20 μL addition each time) aqueous solution of (a) DMA and (b) TMA at room temperature, respectively.

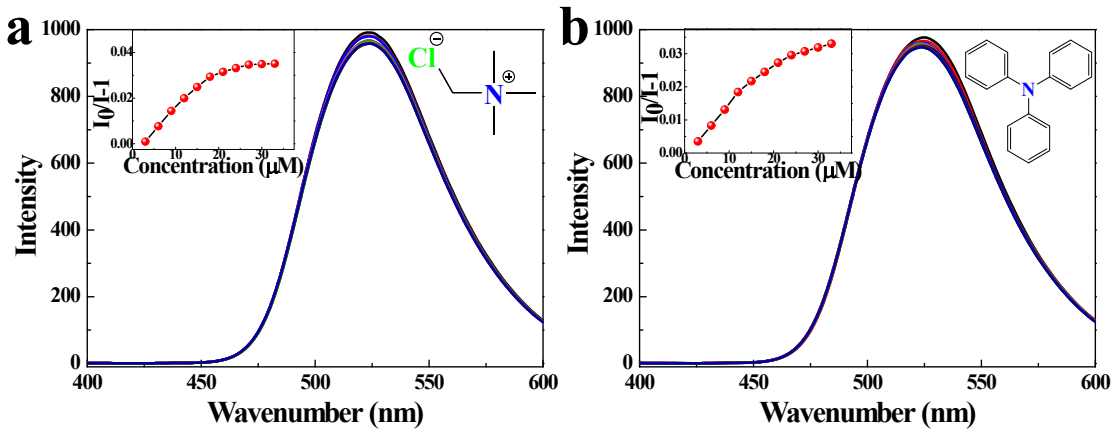

Fig. S16 The emission spectra of F-CTF-3 dispersed in water upon the increased addition of 200 μL (3 μM, 20 μL addition each time) aqueous solution of (a) TMAC and (b) TPA at room temperature, respectively.

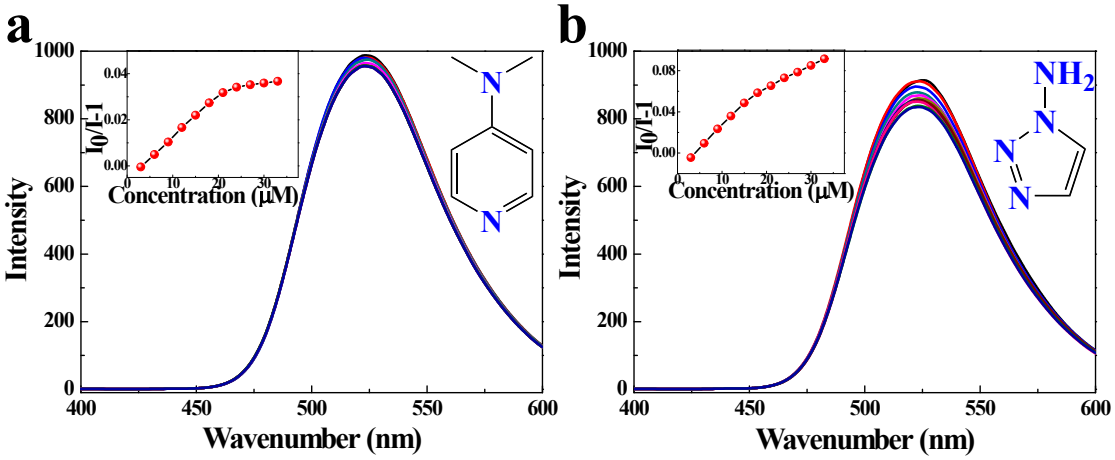

Fig. S17 The emission spectra of F-CTF-3 dispersed in water upon the increased addition of 200 μL (3 μM, 20 μL addition each time) aqueous solution of (a) DMAP and (b) ATL at room temperature, respectively.

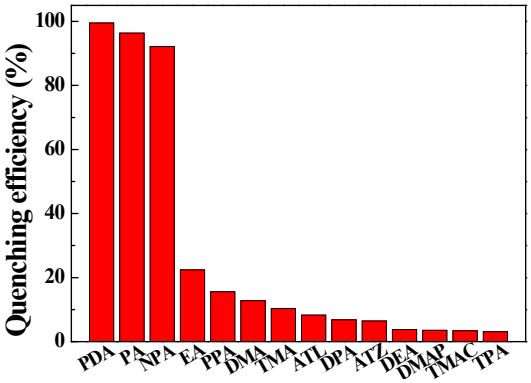

Fig. S18 Fluorescence quenching efficiencies of F-CTF-3 by different analytes at room temperature.

Table S1 The quenching constants (K_{sv}) and limit of detection (LOD) of F-CTF-3 for sensing different analytes at room temperature.

analytes	K_{SV} (F-CTF-3)/M^{-1}	LOD (F-CTF-3)/μM
PDA	6.36×10^{6}	1.47×10^{-3}
PA	8.01×10^{5}	1.17×10^{-2}
NPA	3.57×10^{5}	2.62×10^{-2}
EA	8.76×10^{3}	1.07
PPA	5.59×10^{3}	1.67
DMA	4.44×10^{3}	2.10
TMA	3.50×10^{3}	2.67
ATL	2.74×10^{3}	3.41
DPA	2.23×10^{3}	4.20
ATZ	2.08×10^{3}	4.48
DEA	1.19×10^{3}	7.84
DMAP	1.11×10^{3}	8.39
TMAC	1.07×10^{3}	8.76

TPA	9.77×10^2	9.56	

Table S2 The Stern-Volmer constant (K_{sv}) and limit of detection (LOD) of F-CTF-3 for PA detection was compared with those of other materials.

No.	Material	Solvent/supported systems	LOD (nM)	Ref.
1	FJU-10	DMF	580	*7*
2	dye@FJU-10	DMF	620	*7*
3	Compound 4	Water	6800	*8*
4	Compound 6	Water	9000	*8*
5	LVMOF-1	Water	55	*9*
6	DTPP	THF	12.65	*10*
7	PVDF-Embedded 1	amine vapor	24	*11*
8	phenoxyquinone 1	Acetonitrile	1200	*12*
9	EDMAYM	Acetonitrile	25000	*13*
10	DSB-dialdehyde	Water/THF (9:1)	3760	*14*
11	HPQ-Ac	amine vapor	29000	*15*
12	PFPE-COOH	DMF	90000	*16*
13	Spiropyran derivatives	THF	100	*17*
14	BODIPY derivatives	THF	3060	*18*
15	TPPA	amine vapor	3000000	*19*
16	compounds 1	DMF	3060	*20*
17	compounds 5	DMF	2290	*20*
18	R6G@ZIF-8	acetone	5000000	*21*
19	Film 1	amine vapor	161	*22*

20	8FP-2F	aniline vapor	32.3	*23*
21	S-NG/GCE	water	23	*24*
22	DOF	amine vapor	142	*25*
23	TCbzBSF	amine vapor	60	*26*
24	CDs-silica aerogel	amine vapor	834408	*27*
25	Cellulose-based sensor Phen-MDI-CA	aniline	460	*28*
26	**F-CTF-3**	**water**	**11.7**	***This work***

Table S3 The Stern-Volmer constant (K_{sv}) and limit of detection (LOD) of F-CTF-3 for PDA detection was compared with those of other materials.

No.	**Material**	**Solvent/supported systems**	**LOD (nM)**	**Ref.**
1	PFPE-COOH	DMF	89250	*16*
2	S-NG/GCE	water	51	*24*
3	BCP-Py-CHO	water	7	*29*
4	Py-CHO	water	9000	*29*
5	Gelator	DMSO/H2O (10/1, v/v)	90	*30*
6	ARS/4-FPBA	water	30000	*31*
7	CDs@NBD	water	56	*32*
8	GCE	water	163	*33*
9	DTAF	water	50	*34*
10	**F-CTF-3**	**water**	**1.47**	***This work***

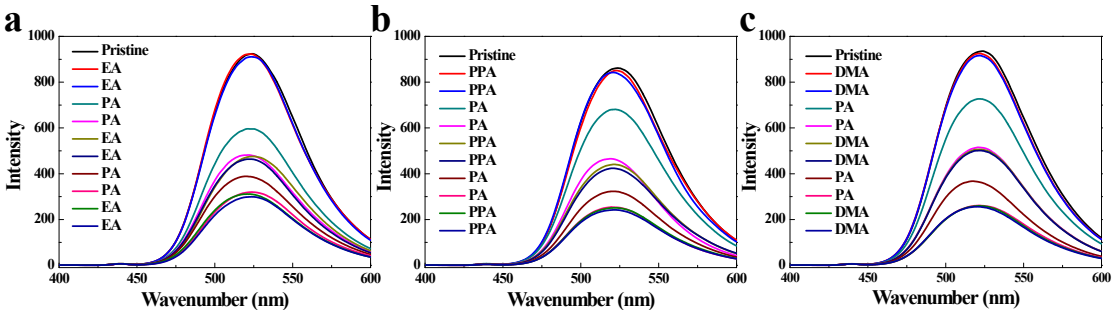

Fig. S19 Tracked emission spectra of F-CTF-3 upon the addition of a saturated aqueous solution of (a) EA, (b) PPA and (c) DMA followed by 3 μM aqueous solution of PA at room temperature, respectively (20 μL addition each time).

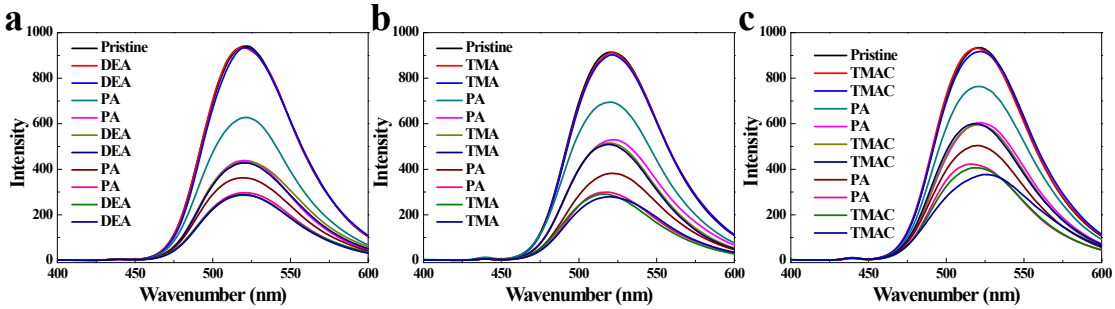

Fig. S20 Tracked emission spectra of F-CTF-3 upon the addition of a saturated aqueous solution of (a) DEA, (b) TMA and (c) TMAC followed by 3 μM aqueous solution of PA at room temperature, respectively (20 μL addition each time).

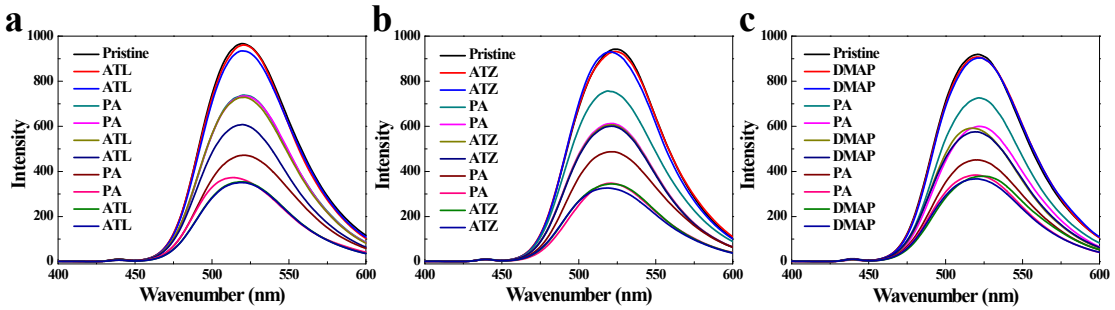

Fig. S21 Tracked emission spectra of F-CTF-3 upon the addition of a saturated aqueous solution of (a) ATL, (b) ATZ and (c) DMAP followed by 3 μM aqueous solution of PA at room temperature, respectively (20 μL addition each time).

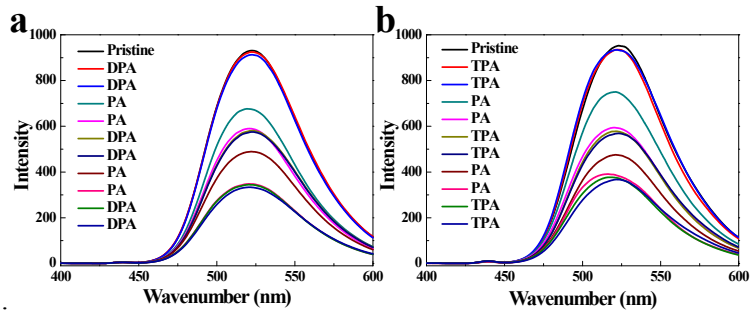

Fig. S22 Tracked emission spectra of F-CTF-3 upon the addition of a saturated aqueous solution of (a) DPA and (c) TPA followed by 3 μM aqueous solution of PA at room temperature, respectively (20 μL addition each time).

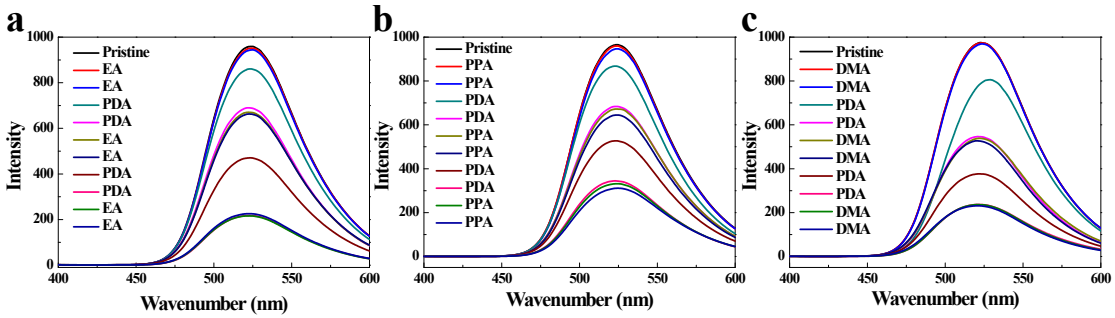

Fig. S23 Tracked emission spectra of F-CTF-3 upon the addition of a saturated aqueous solution of (a) EA, (b) PPA and (c) DMA followed by 3 μM aqueous solution of PDA at room temperature, respectively (20 μL addition each time).

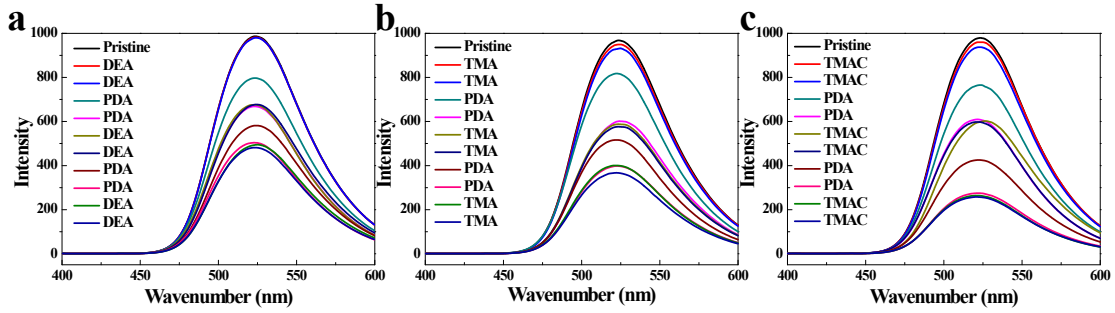

Fig. S24 Tracked emission spectra of F-CTF-3 upon the addition of a saturated aqueous solution of (a) DEA, (b) TMA and (c) TMAC followed by 3 μM aqueous solution of PDA at room temperature, respectively (20 μL addition each time).

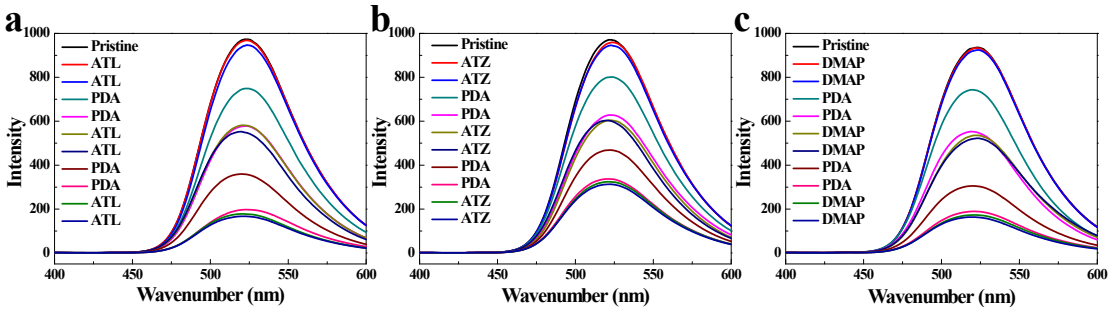

Fig. S25 Tracked emission spectra of F-CTF-3 upon the addition of a saturated aqueous solution of (a) ATL, (b) ATZ and (c) DMAP followed by 3 μM aqueous solution of PDA at room temperature, respectively (20 μL addition each time).

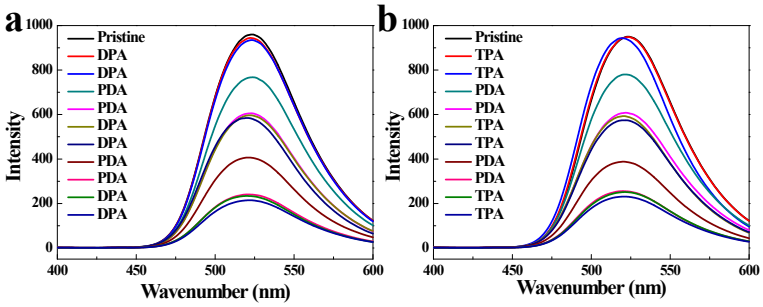

Fig. S26 Tracked emission spectra of F-CTF-3 upon the addition of a saturated aqueous solution of (a) DPA and (c) TPA followed by 3 μM aqueous solution of PDA at room temperature, respectively (20 μL addition each time).

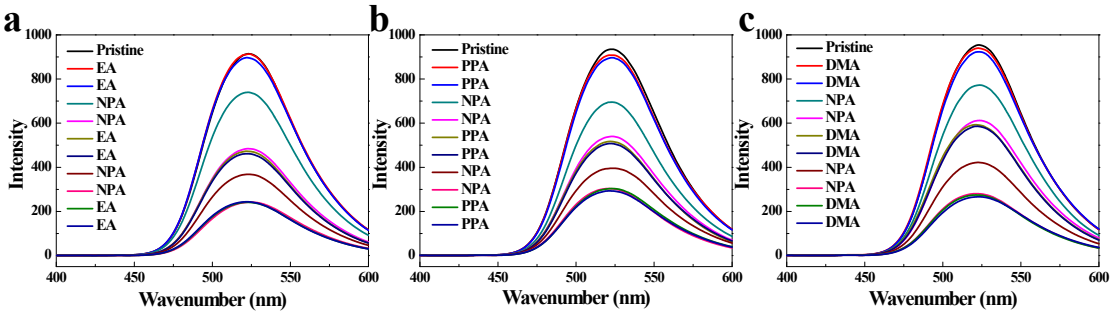

Fig. S27 Tracked emission spectra of F-CTF-3 upon the addition of a saturated aqueous solution of (a) EA, (b) PPA and (c) DMA followed by 3 μM aqueous solution of NPA at room temperature, respectively (20 μL addition each time).

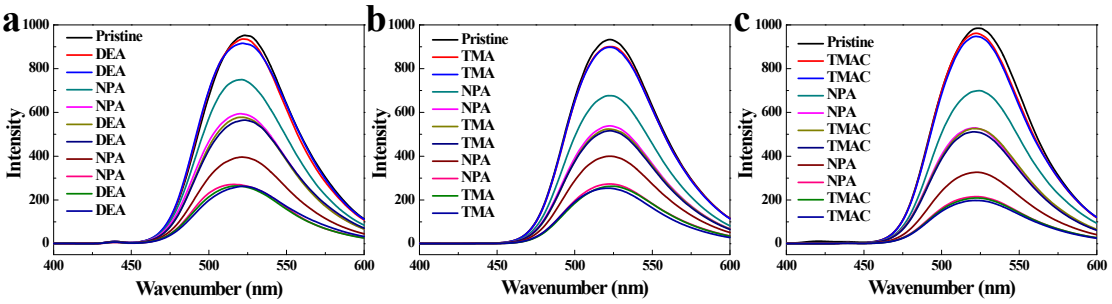

Fig. S28 Tracked emission spectra of F-CTF-3 upon the addition of a saturated aqueous solution of (a) DEA, (b) TMA and (c) TMAC followed by 3 μM aqueous solution of NPA at room temperature, respectively (20 μL addition each time).

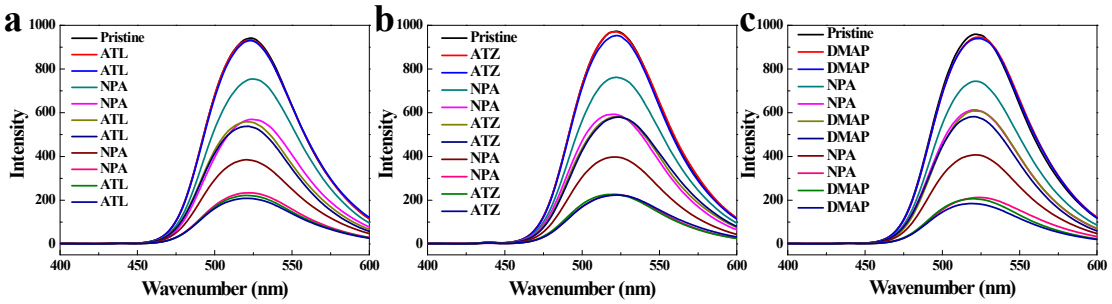

Fig. S29 Tracked emission spectra of F-CTF-3 upon the addition of a saturated aqueous solution of (a) ATL, (b) ATZ and (c) DMAP followed by 3 μM aqueous solution of NPA at room temperature, respectively (20 μL addition each time).

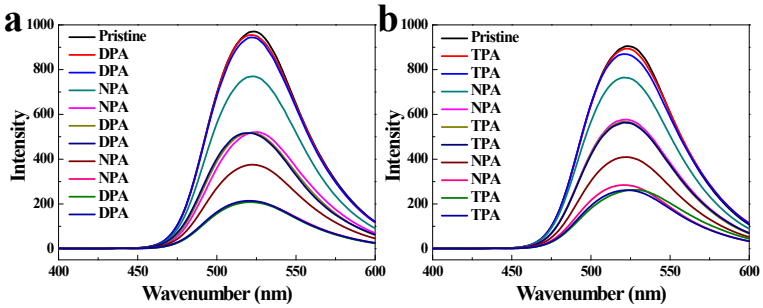

Fig. S30 Tracked emission spectra of F-CTF-3 upon the addition of a saturated aqueous solution of (a) DPA and (c) TPA followed by 3 μM aqueous solution of NPA at room temperature, respectively (20 μL addition each time).

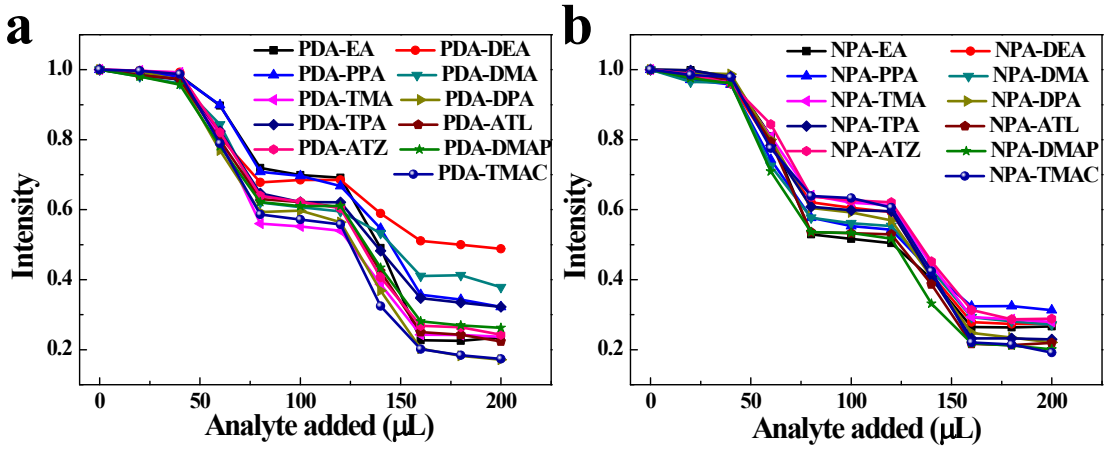

Fig. S31 Selective detection of (a) PDA and (b) NPA on F-CTF-3 in the presence of the other non-PAAs in water at room temperature.

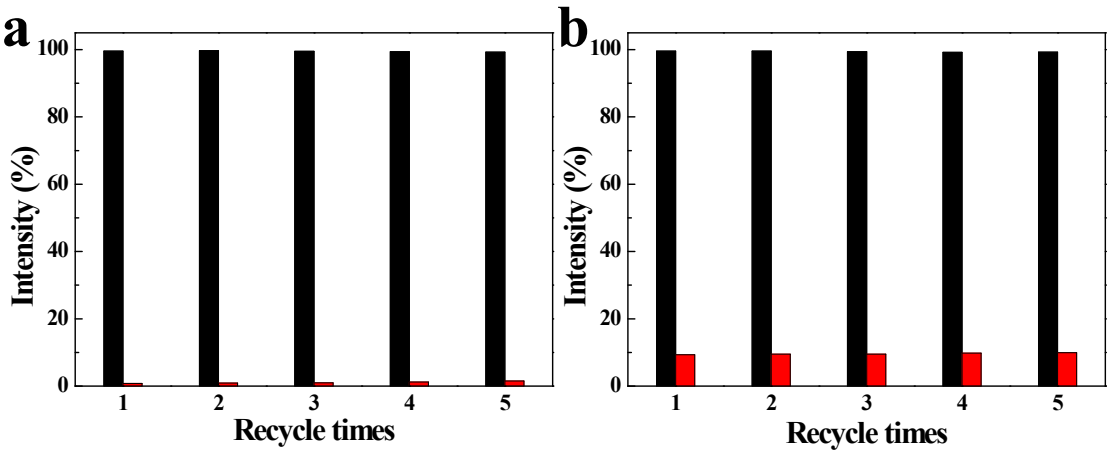

Fig. S32 The recycle stability F-CTF-3 for (a) PDA and (b) NPA detection at room temperature. (The black bars represent the initial fluorescence intensity and the red bars represent the intensity upon addition a solution of 2 mL 30 μM analyte PDA or NPA in water).

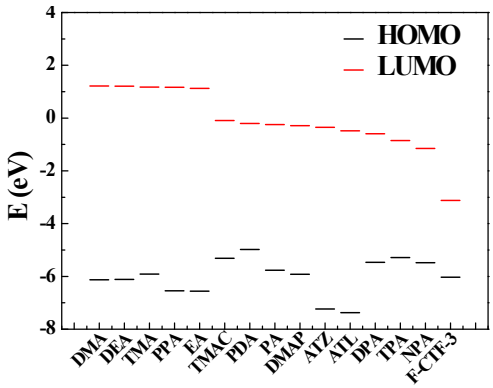

Fig. S33 (b) HOMO and LUMO energies for selected analytes and F-CTF-3 arranged in decreased order of LUMO energies.

Table S4 HOMO and LUMO energies calculated for selected analytes and F-CTF-3 used at B3LYP/6-31G* level.

Analytes	HUMO (ev)	LUMO (ev)	Band Gap (ev)
DMA	-6.12801	1.21281	7.34082
DEA	-6.11712	1.20683	7.32395
TMA	-5.91304	1.17199	7.08503
PPA	-6.54706	1.16601	7.71307
EA	-6.55604	1.12546	7.6815
TMAC	-5.30976	-0.09034	5.21942
PDA	-4.98186	-0.2049	4.77696
PA	-5.76555	-0.24871	5.51684
DMAP	-5.91576	-0.28953	5.62623
ATZ	-7.23333	-0.3532	6.88013
ATL	-7.37157	-0.48083	6.89074
DPA	-5.46405	-0.59539	4.86866
TPA	-5.28799	-0.85281	4.43518
NPA	-5.47711	-1.15295	4.32416
F-CTF-3	-6.027	-3.123	2.904

Table S5. Stern–Volmer quenching constants and bimolecular quenching constant for the interaction of F-CTF-3 and different analytes.

Analyte	K_{sv} (M^{-1}) (0°C)	K_{sv} (M^{-1}) (25°C)	K_q (mol/s)
PDA	2.62×10^{7}	6.36×10^{6}	3.81×10^{15}
PA	1.82×10^{6}	8.01×10^{5}	4.80×10^{14}
NPA	8.33×10^{5}	3.57×10^{5}	2.14×10^{14}

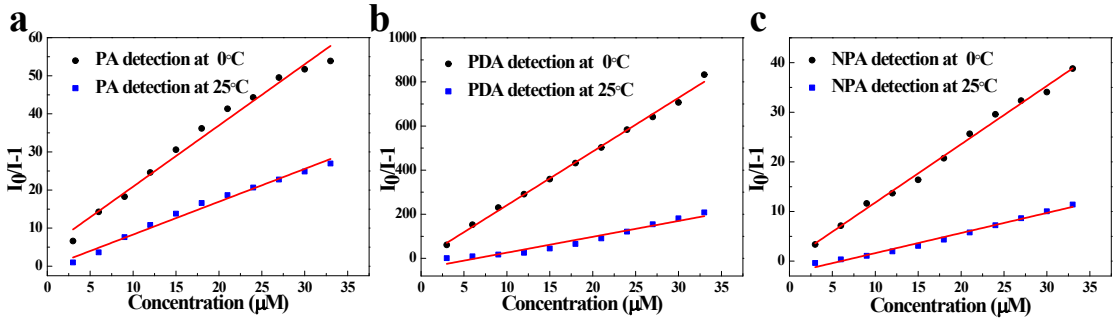

Fig. S34 The SV plots of the selected PAAs (a. PA, b. PDA and c. NPA) (3 uM, 20 μL each time) in F-CTF-3 suspension solution at different temperature.

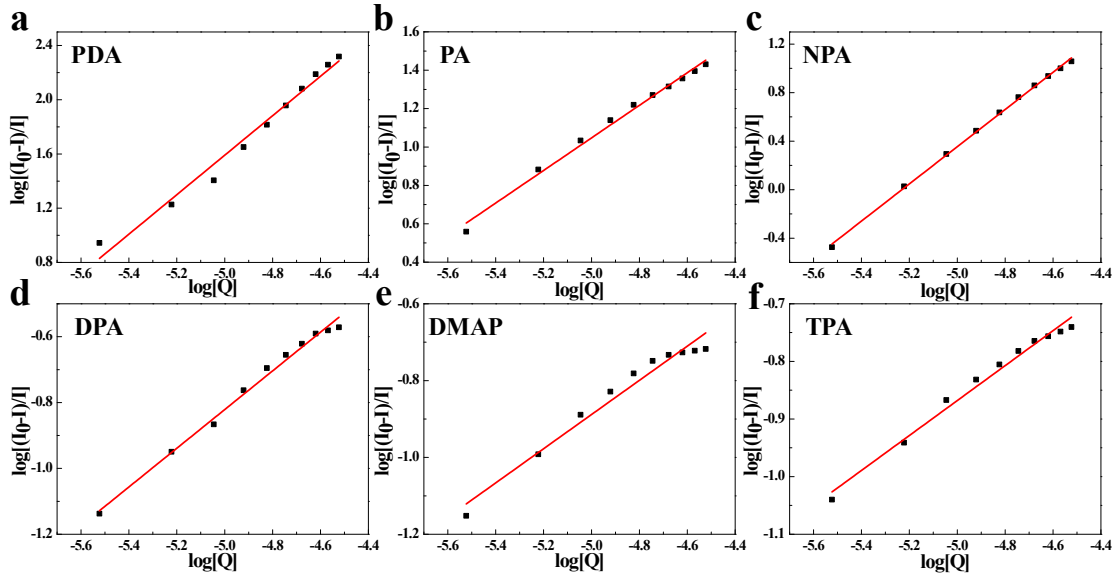

Fig. S35 Plot of $\log[(I_0\text{-}I)/I]$ versus $\log[Q]$ for the interaction of (a) PDA, (b) PA, (c) NPA, (d) DPA, (e) DMAP and (f) TPA with F-CTF-3 in aqueous solution.

Table. S6 binding parameters for the interaction of F-CTF-3 and different analytes.

Analyte	K_b (L/mol)	n
PDA	7.45×10^{8}	1.54
PA	1.06×10^{7}	1.46
NPA	1.95×10^{6}	1.08
DPA	1.31×10^{2}	0.59
DMAP	2.17×10^{1}	0.45
TPA	4.45×10^{0}	0.31

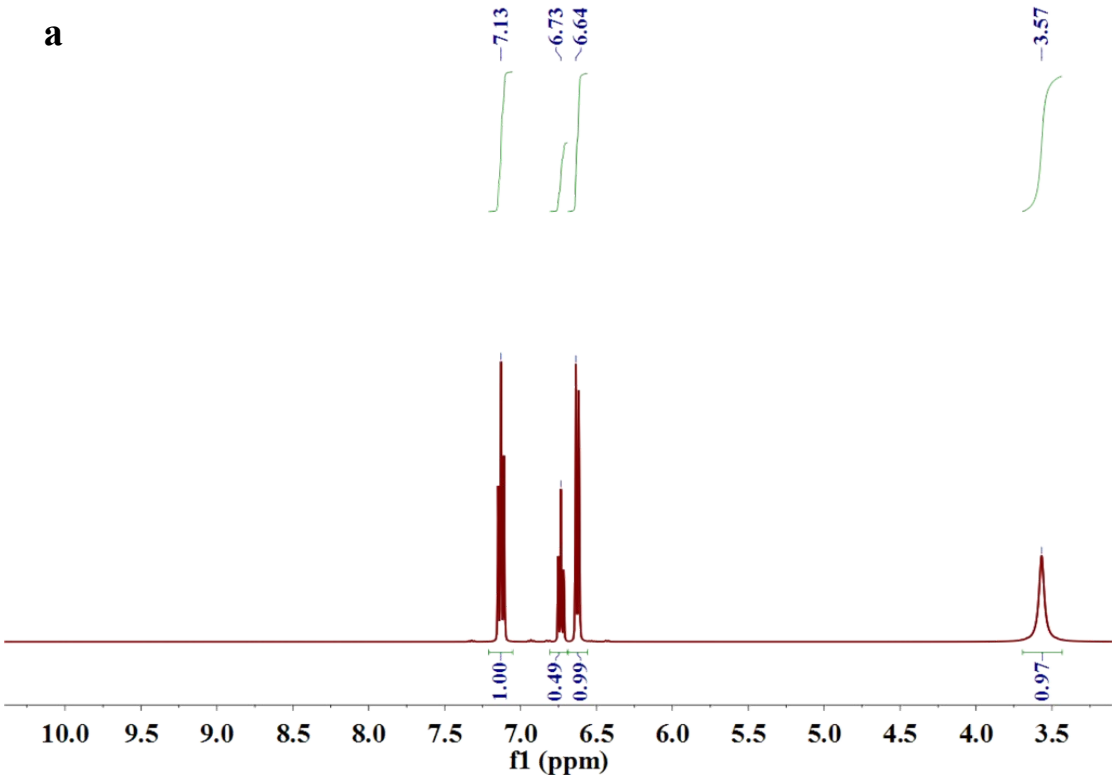

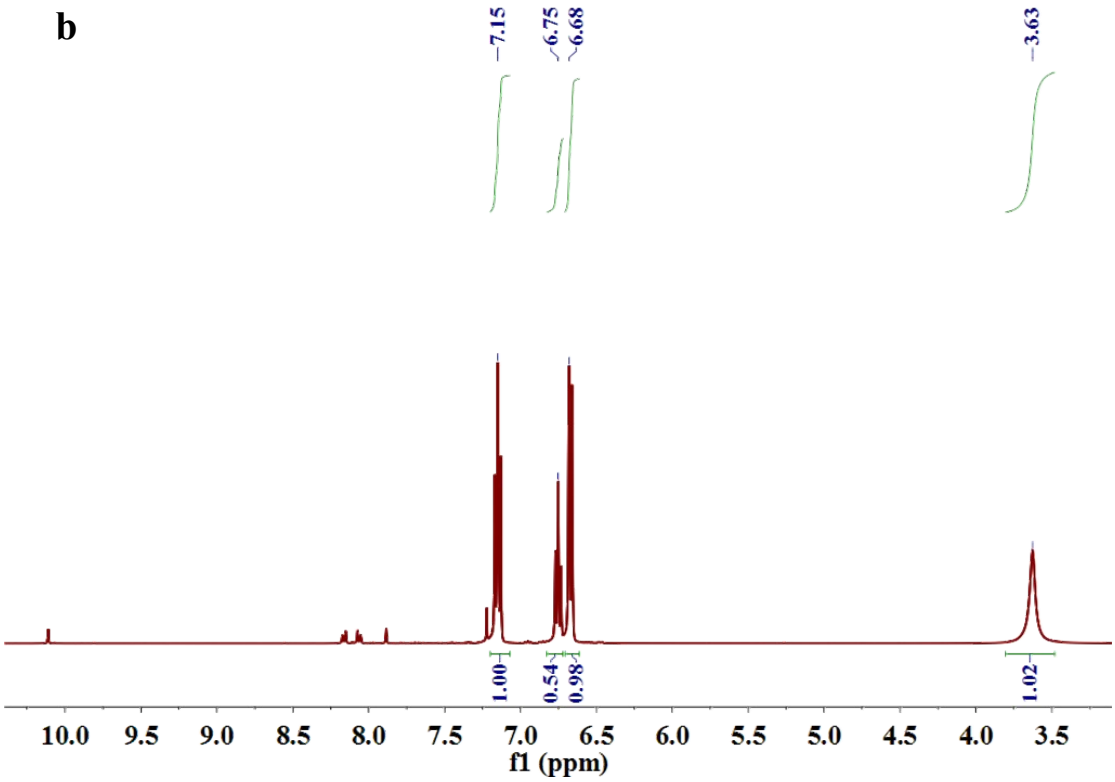

Fig. S36. ^{1}H NMR spectra of (a) PA and (a) PA@BTDD.

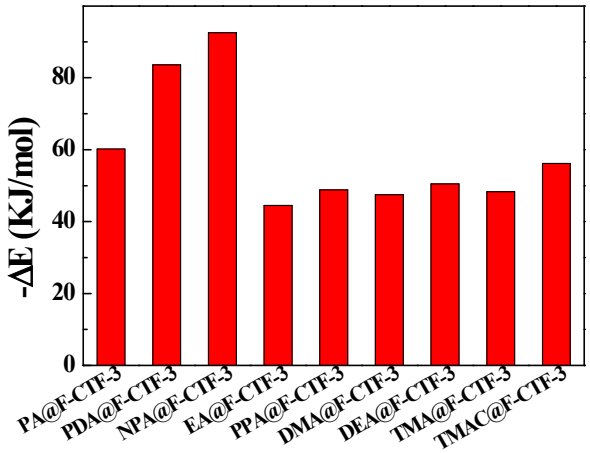

Fig. S37 The binding energies of PAAs and various aliphatic amines on F-CTF-3.

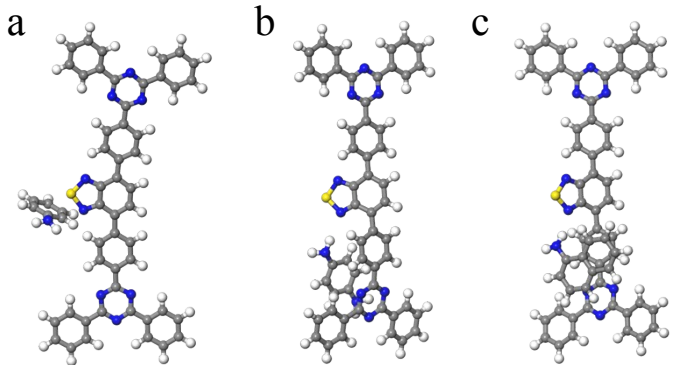

Fig. S38 Optimized geometries for the interactions of F-CTF-3 with (a) PA, (b) PDA and (c) NPA. Color code: C, gray; H, white; N, blue; S, yellow.

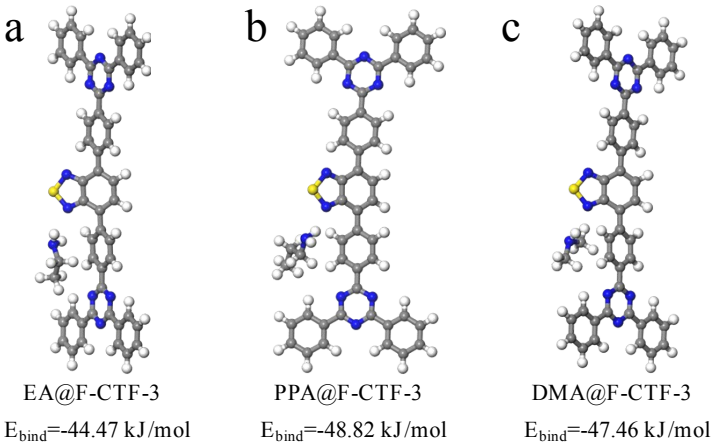

Fig. S39 Optimized geometries for the interactions of F-CTF-3 with (a) EA, (b) PPA and (c) DMA. Color code: C, gray; H, white; N, blue; S, yellow.

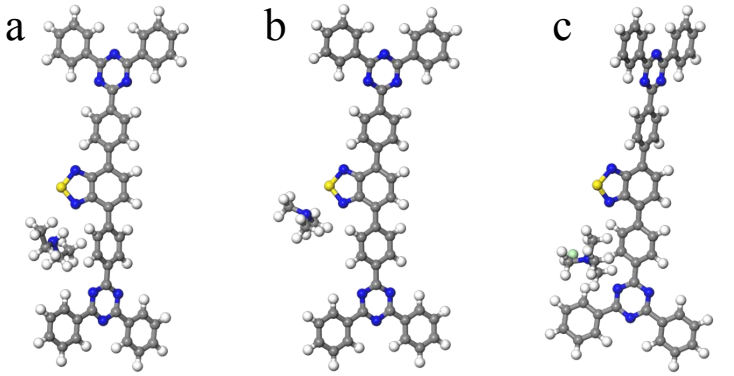

Fig. S40 Optimized geometries for the interactions of F-CTF-3 with (a) DEA, (b) TMA and (c) TMAC. Color code: C, gray; H, white; N, blue; S, yellow; Cl, reseda.

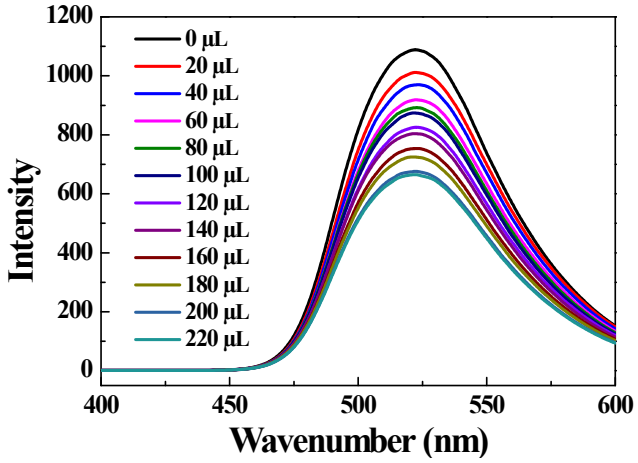

Fig. S41 The emission spectra of F-CTF-3 dispersed in water upon incremental addition of triaminobenzene (TAB) (3 μM, 20 μL addition each time). The TAB solution was neutralized with NaOH before fluorescence detection experiments.

Table S7. The quenching constants (K_{sv}) and limit of detection (LOD) of F-CTF-3 for sensing different analytes at room temperature.

analytes	K_{SV} (F-CTF-3)/M^{-1}	LOD (F-CTF-3)/μM
PDA	6.36×10^{6}	1.47×10^{-3}
PA	8.01×10^{5}	1.17×10^{-2}
NPA	3.57×10^{5}	2.62×10^{-2}
TAB[a]	2.13×10^{4}	4.40×10^{-1}

[a] TAB solution was neutralized before the fluorescence quenching experiment.

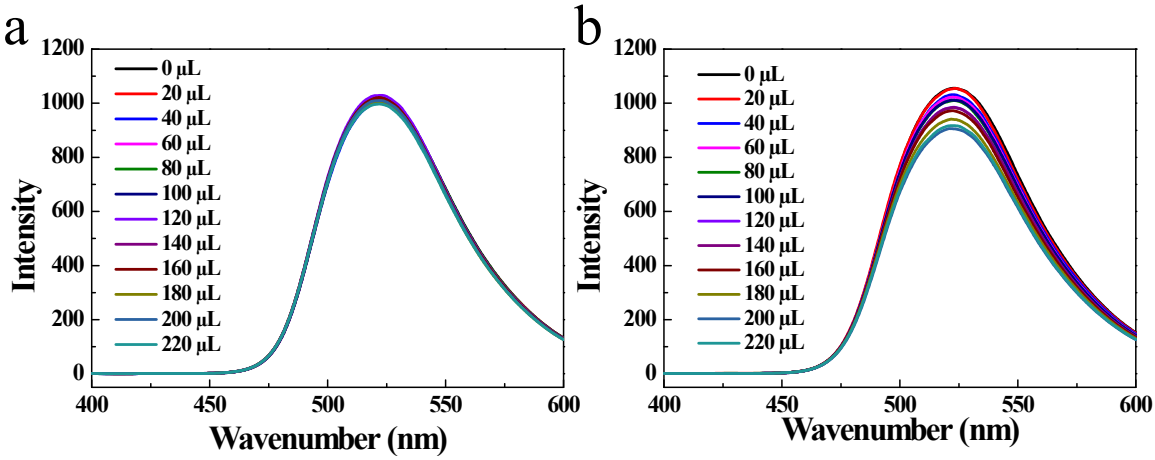

Fig. S42 The emission spectra of F-CTF-3 dispersed in water upon incremental addition of (a) PA and (b) TAB in pH=1 aqueous solution (3 μM, 20 μL addition each time).

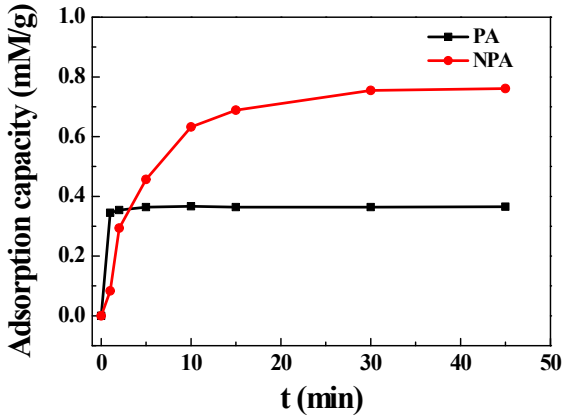

Fig. S43 Adsorption kinetics of F-CTF-3 after adsorbed PA and NPA. (The initial concentration is 0.5 mM)

The adsorption dates fitting by kinetic models

In order to get more information about sorption process, the experimental dates were fitted with the pseudo-first-order kinetic model and the pseudo-second-order kinetic model. Two models are expressed as follows.

The pseudo-first-order equation:

$$\ln(Q_e - Q_t) = \ln Q_e - k_1 t$$

The pseudo-second-order equation:

$$\frac{\mathrm{t}}{\mathrm{Q_t}} = \frac{1}{k_2 Q_e^2} + \frac{t}{Q_e}$$

Where Q_t (mM g^{-1}) and Q_e (mM g^{-1}) are sorption quantity of PA and NPA at time t and at equilibrium, K_1 (min^{-1}) and K_2 (g $mM^{-1}min^{-1}$) are the pseudo-first-order and pseudo-second-order equation rate constants. The plots of ln (Q_e-Q_t) versus t and t/Q_t versus t are shown in Fig. S44. The model parameters and the correlation coefficients are listed in Table S8.

Table S8 The kinetic parameters for the PA and NPA adsorption on F-CTF-3.

	pseudo-first-order kinetic model			pseudo-second-order kinetic model		
	Q_e(mM g^{-1})	k_1(min^{-1})	R_2	Q_e(mM g^{-1})	k_2 (g mM^{-1} min^{-1})	R_2
F-CTF-3-PA	0.2430	0.74799	0.80585	0.3694	34.53457	0.99999
F-CTF-3-NPA	0.6252	0.10829	0.95215	0.8561	0.30048	0.99997

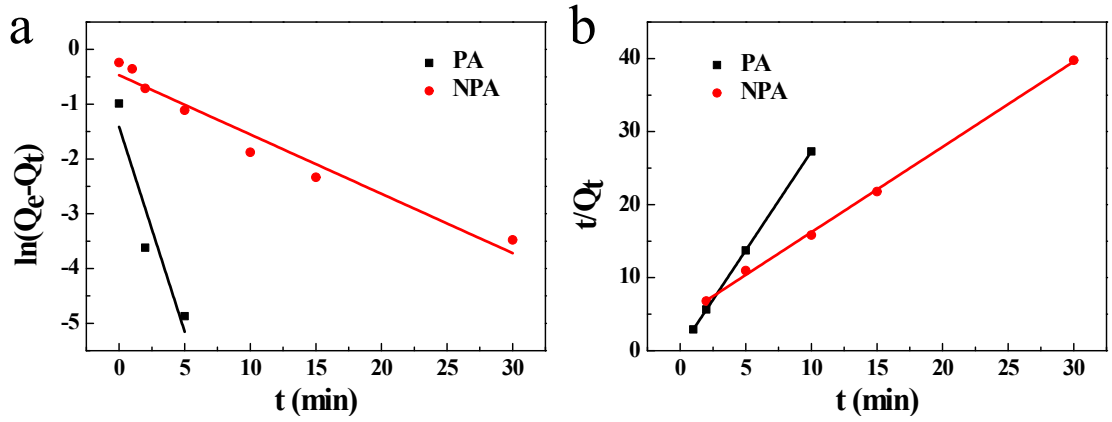

Fig. S44 The pseudo-first-order kinetic model (a) and pseudo-second-order kinetic model (b) linearized plots for PA and NPA adsorption on F-CTF-3.

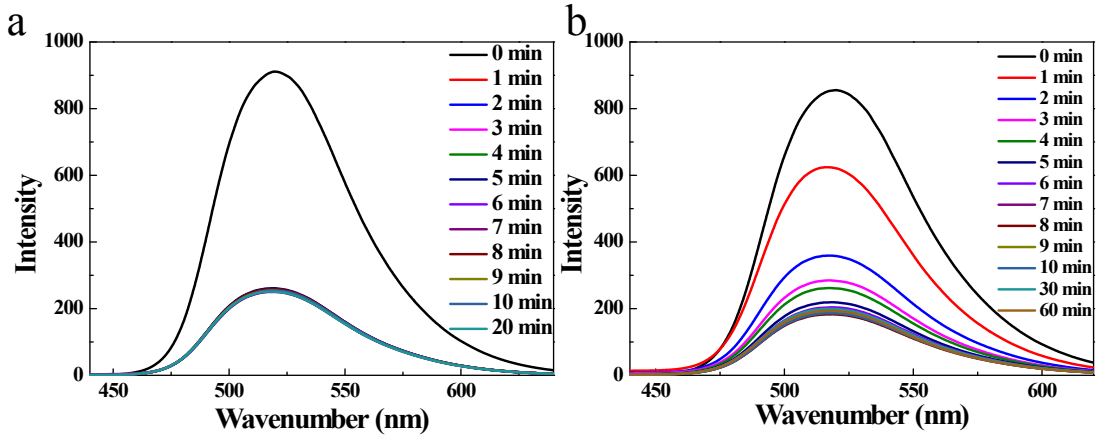

Fig. S45 The emission spectra of F-CTF-3 dispersed in water after adding (a) PA and (b) NPA solution with the increasingly time.

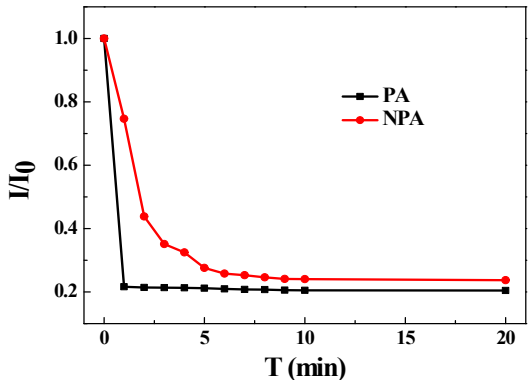

Fig. S46 The time-depended emission spectra intensity of F-CTF-3 suspension towards (a) PA and (b) NPA.

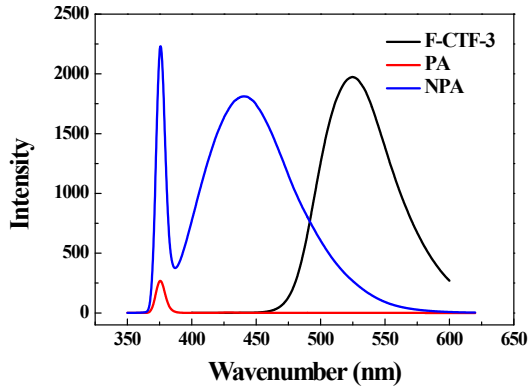

Fig. S47 The emission spectra of PA, NPA and F-CTF-3 dispersed in water system.

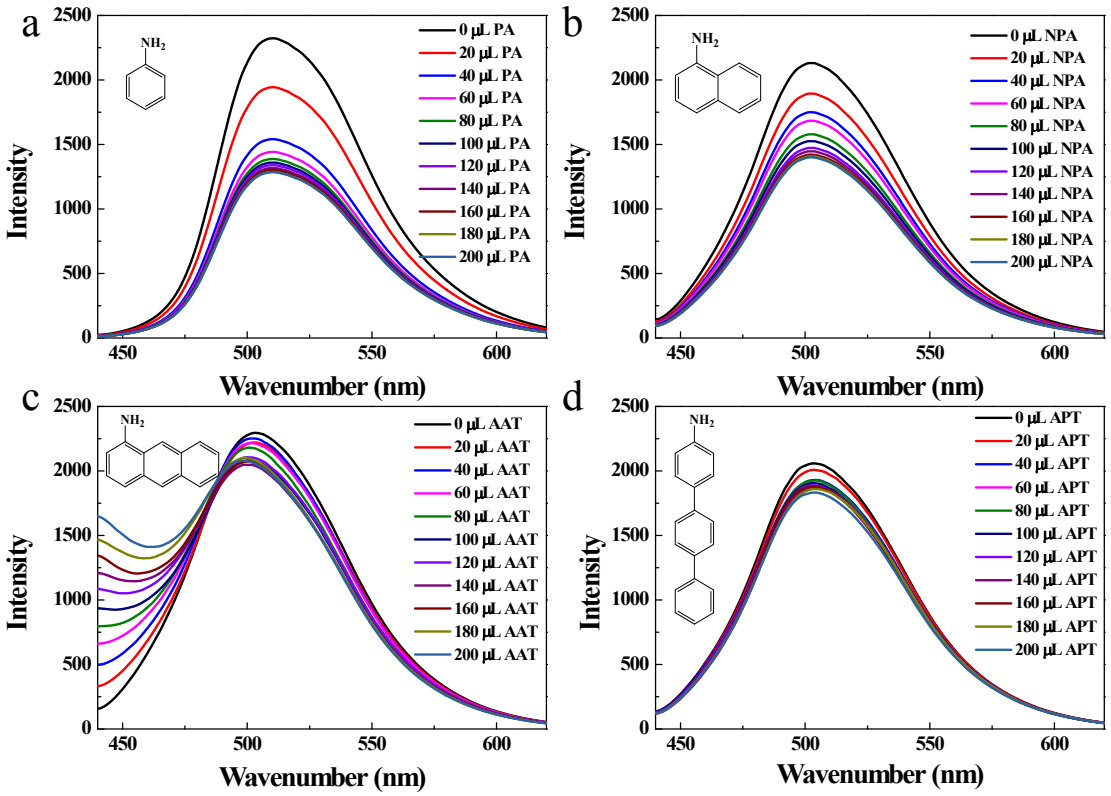

Fig. S48 The emission spectra of F-CTF-3 dispersed in DMF system upon incremental addition of four amines (a. PA, b. NPA, c. AAT and d. APT) (3 μM, 20 μL each time).

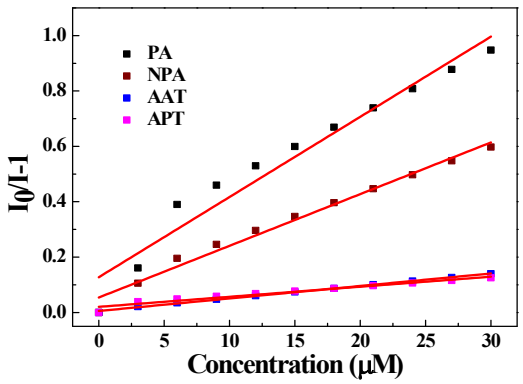

Fig. S49 The SV plots of the selected amines (PA, NPA, AAT and APT) (3 μM, 20 μL each time) in F-CTF-3 suspension solution.

Table S9 The quenching constants (K_{sv}) of F-CTF-3 for sensing different molecule size analytes.

analytes	K_{SV} (F-CTF-3)/M^{-1}
PA	2.69×10^4
NPA	1.74×10^4
AAT	4.22×10^3
APT	4.13×10^3

References

[1] Y. Z. Tang, H. L. Huang, W. J. Xue, Y. J. Chang, Y. Li, X. Y. Guo, C. L. Zhong, Rigidifying induced fluorescence enhancement in 2D porous covalent triazine framework nanosheets for the simultaneously luminous detection and adsorption removal of antibiotics, *Chem. Eng. J*., 2020, 384,123382.

[2] M. Y. Liu, Q. Huang, S. L. Wang, Z. Y. Li, B. Y. Li, S. B. Jin and B. E. Tan, *Angew. Chem. Int. Ed.*, **2018**, *130*, 12144-12148.

[3] W. J. Luo, Y. X. Zhu, J. Y. Zhang, J. J. He, Z. G. Chi, P. W. Miller, L. P. Chen and C. Y. Su, *Chem. Commun.,* 2014, **50***,* 11942-11945.

[4] J. N. Hao and B. Yan, *Chem. Commun.,* 2015, **51**, 7737-7740.

[5] P. Mandal, D. Sahoo, P. Sarkar, K. Chakrabortyd and S. Das, Fluorescence turn-on and turn-off sensing of pesticides by carbon dot-based sensor, *New J. Chem.*, **2019**, *43*, 12137-12151.

[6] Y. Li, F. Gao, F. Gao, F. Shan, J. Bian, C. Zhao, Study on the Interaction between 3 Flavonoid Compounds and α-Amylase by Fluorescence Spectroscopy and Enzymatic Kinetics, *J. Food. Sci.*, **2009**, *74*, 199-203.

[7] L. Z. Liu, Z. Z. Yao, Y. X. Ye, C. L. Liu, Q. J. Lin, S. M. Chen, S. C. Xiang, Z. J. Zhang, Enhancement of Intrinsic Proton Conductivity and Aniline Sensitivity by Introducing Dye Molecules into the MOF Channel, *ACS Appl. Mater. Interfaces,* **2019**, *11*, 16490−16495.

[8] H. J. Feng, L. Xua, B. Liu, H. Jiao, Europium Metal-Organic Frameworks as Recyclable and Selective Turn-off Fluorescence Sensors for Aniline Detection, *Dalton Trans.*, **2016**, *45*, 17392-17400.

[9] T. Gong, P. Li, Q. Sui, J. Q. Chen, J. H. Xu, E. Q. Gao, Stable electron-deficient metal-organic framework for colorimetric and luminescent sensing of phenols and anilines, *J. Mater. Chem. A*, **2018**, *6*, 9236-9244.

[10] U. Balijapalli, S. Manickam, K. Thirumoorthy, K. N. Sundaramurthy, K. I. Sathiyanarayanan, (Tetrahydrodibenzo[*a,i*]phenanthridin-5-yl)phenol as a Fluorescent Probe for the Detection of Aniline, *J. Org. Chem.*, **2019**, *84*, 11513−11523.

[11] B. P. Jiang, D. S. Guo, Y. Liu, Reversible and Selective Sensing of Aniline Vapor by Perylene-Bridged Bis(cyclodextrins) Assembly, *J. Org. Chem.*, **2011**, *76*, 6101–6107.

[12] I. S. Park, E. Heo, Y. S. Nam, C. W. Lee, J. M. Kim, Colorimetric detection of aliphatic primary amines and a molecular logic gate based on a photochromic phenoxyquinone derivative, *J. Photoch. Photobio. A*, **2012**, *238*, 1–6.

[13] A. R. Longstreet, M. Jo, R. R. Chandler, K. Hanson, N. Zhan, J. J. Hrudka, H. Mattoussi, M. Shatruk, D. T. McQuade, Ylidenemalononitrile Enamines as Fluorescent "Turn-On" Indicators for Primary Amines, *J. Am. Chem. Soc*., **2014**, *136*, 15493−15496.

[14] J. Kumpf, S. T. Schwaebel, U. H. F. Bunz, Amine Detection with Distyrylbenzenedialdehyde-Based Knoevenagel Adducts, *J. Org. Chem.,* **2015**, *80*, 5159−5166.

[15] M. Gao, S. W. Li, Y. H. Lin, Y. Geng, X. Ling, L. C. Wang, A. J. Qin, B. Z. Tang, Fluorescent Light-Up Detection of Amine Vapors Based on Aggregation-Induced Emission, *ACS Sens.*, **2016**, *1*, 179−184.

[16] Y. J. Zhao, K. S. Miao, Z. T. Zhu, L. J. Fan, Fluorescence Quenching of a Conjugated Polymer by Synergistic Amine-Carboxylic Acid and π−π Interactions for Selective Detection of Aromatic Amines in Aqueous Solution, *ACS Sens.*, **2017**, *2*, 842−847.

[17] W. G. Tian, Y. N. Xue, J. T. Tian, P. Z. Gong, J. H. Dai, X. Wang, Z. B. Zhu, Colorimetric and fluorometric dual-mode detection of aniline pollutants based on spiropyran derivatives, *RSC Adv.*, **2016**, *6*, 83312–83320.

[18] Y. Y. Fu, Q. G. He, D. F. Zhu, Y. R. Wang, Y. X. Gao, H. M. Cao, J. G. Cheng, A BODIPY dye as a reactive chromophoric/fluorogenic probe for selective and quick detection of vapors of secondary amines, *Chem. Commun.*, **2013**, *49*, 11266-11268.

[19] T. Y. Han, J. W. Y. Lam, N. Zhao, M. Gao, Z. Y. Yang, E. G. Zhao, Y. P. Dong, B. Z. Tang, A fluorescence-switchable luminogen in the solid state: a sensitive and selective sensor for the fast "turn-on" detection of primary amine gas, *Chem. Commun.*, **2013**, *49*, 4848-4850.

[20] J. F. Song, H. F. Wen, J. J. Luo, Y. Y. Jia, X. Y. Zhang, L. J. Su, R. S. Zhou, Five isomorphic lanthanide metal-organic frameworks constructed from 5-(3-carboxy-phenyl)-pyridine-2-carboxylic acid and oxalate: Synthesis, crystal structures and selective fluorescence sensing for aniline, *J. Solid State Chem.*, **2019**, *269*, 43–50.

[21] T. T. Han, J. Yang, Y. Y. Liu, J. F. Ma, Rhodamine 6G loaded zeolitic imidazolate framework-8 (ZIF-8) nanocomposites for highly selective luminescent sensing of Fe^{3+}, Cr^{6+} and aniline, *Micropor. Mesopor. Mat.*, **2016**, *228*, 275-288.

[22] C. D. Shang, G. Wang, M. X. He, X. M. Chang, J. Y. Fan, K. Q. Liu, H. N. Peng, Y. Fang, A high performance fluorescent arylamine sensor toward lung cancer Sniffing, *Sensor Actuat. B-Chem.*, **2017**, *241*, 1316–1323.

[23] Z. N. Jiao, Y. Zhang, W. Xu, X. T. Zhang, H. B. Jiang, P. C. Wu, Y. Y. Fu, Q. G. He, H. M. Cao, J. G. Cheng, Highly Efficient Multiple-Anchored Fluorescent Probe for the Detection of Aniline Vapor Based on Synergistic Effect: Chemical Reaction and PET, *ACS Sens.*, **2017**, *2*,

687−694.

[24] W. Q. Zhu, J. J. Gao, H. O. Song, X. Z. Lin, S. P. Zhang, Nature of synergistic effect of N and S co-doped graphene for enhanced simultaneous determination of toxic pollutants, *ACS Appl. Mater. Interfaces*, **2019**, *11*, 44545−44555.

[25] H. Su, R. Liu, M. L. Shu, M. Tang, J. Wang, H. J. Zhu, Fluorenone-based organogel and self-assembled fbrous flm: Synthesis, optical properties and reversible detection of aniline vapor, *Dyes Pigments*, **2019**, *162*, 52–58.

[26] L. Zhai, Y. H. Shu, J. B. Sun, M. Sun, Y. Y. Song, R. Lu, Spirofluorene-Cored Difluoroboron β-Diketonate Complexes with Terminal Carbazole: Synthesis, Self-Assembling, and Fluorescent Sensory Properties, *Eur. J. Org. Chem.*, **2019**, 3093–3100.

[27] Y. S. Ma, X. Chen, J. L. Bai, G. J. Yuan, L. L. Ren, Highly selective fluorescence chemosensor based on carbon-dot-aerogel for detection of aniline gas, *Inorg. Chem. Commun.*, **2019**, *100*, 64–69.

[28] H. Nawaz, J. M. Zhang, W. G. Tian, K. F. Jin, R. N. Jia, T. T. Yang, J. Zhang, Cellulose-based fluorescent sensor for visual and versatile detection of amines and anions, Journal of Hazardous Materials, **2020**, *387*, 121719.

[29] L. F. Gao, X. Lin, X. Hai, X. W. Chen, J. H. Wang, Polymeric Ionic Liquid-Based Fluorescent Amphiphilic Block Copolymer Micelle for Selective and Sensitive Detection of *p*-Phenylenediamine, *ACS Appl. Mater. Interfaces*, **2018**, *10*, 43049−43056.

[30] X. H. Cao, N. Zhao, A. P. Gao, H. T. Lv, Y. L. Jia, R. M. Wu, Y. Q. Wu, Bis-naphthalimides self-assembly organogel formation and application in detection of *p*-phenylenediamine, *Mat. Sci. Eng. C*, **2017**, *70*, 216–222.

[31] K. Ngamdee, S. Martwiset, T. Tuntulani, W. Ngeontae, Selective fluorescence sensors for *p*-phenylenediamine using formyl boronate ester with an assistance of micelles, *Sensor. Actuat. B-Chem.*, **2012**, *173*, 682–691.

[32] W. J. Wang, J. M. Xia, X. Hai, M. L. Chen, J. H. Wang, A Hybrid of Carbon Dots with 4-Chloro-7-Nitro-1,2,3-Benzoxadiazole for Selective Detection of *p*-Phenylenediamine, *Environ. Sci.: Nano*, **2017**, *4*, 1037-1044.

[33] J. J. Gao, W. Q. Zhu, H. O. Song, S. P. Zhang, Highly-Sensitive Simultaneous Determination of *p*-Phenylenediamine and Hydroquinone by Recognizing Electrochemical Reduction Responses on Bare GCE, *J. Electrochem. Soc.*, **2019**, *166*, 35-41.

[34] H. Y. Ko, Y. H. Lin, C. J. Shih, Y. L. Chen, Determination of phenylenediamines in hair

colors derivatizated with 5-(4,6-dichlorotriazinyl) aminofluorescein via micellar electrokinetic chromatography, *J. Food. Drug. Anal.*, **2019**, *27*, 825-831.